Radiation-Induced Charge Collection in Infrared Detector Arrays

J.C.Pickel, R.A.Reed, R.Ladbury, B.Rauscher, P.W.Marshall, T.M.Jordan, B.Fodness and G.Gee

Abstract*---A modeling approach is described for predicting charge collection in space-based infrared detector arrays due to ionizing particle radiation. The modeling uses a combination of analytical and Monte Carlo techniques to capture the essential features of energetic-ion-induced charge collection to detector pixels in a two-dimensional array. The model addresses several aspects that are necessary for high fidelity simulation of complex focal plane array structures including multiple layers, sub-regions within layers, variation of LET with range, secondary electron scattering, free-field diffusion, and field-assisted diffusion. Example results are given and predictions are compared to experimental data.

1. INTRODUCTION

Optical sensors for space-based imaging missions have evolved toward large two-dimensional arrays of detectors. Significant advances have been made in infrared (IR) detector array and readout integrated circuit (ROIC) technology, with greatly improved sensitivity and reduced noise levels. It is not uncommon to see read noise specifications on the order of 10 electrons or less, concomitant with very long integration times of several hundred to thousands of seconds [1]. With these performance requirements and operation in space, the radiation environment from galactic cosmic rays (GCR), trapped particles and energetic solar particles can dominate the noise in the focal plane array (FPA) pixels. Optical detectors, by design, are efficient sensors of ionization and the single event transients from energetic particles in the space environment are registered in the FPA pixels when they are penetrated by the particles. Shielding is not effective due to the high energies of the particles and due to secondary particle generation when passing through shielding. The particle-induced noise can be mitigated through a variety of signal processing techniques and operational scenarios. For mitigation strategies to be successful, it is necessary to have a high-fidelity predictive model of the charge collection in the detector arrays, particularly the spatial distribution of the particle-induced charge. The problem has become more challenging as the noise levels have been reduced with modern technology and enhanced performance requirements.

Charge generated from single event transients is captured on the integration nodes of detector array pixels and remains until the array is reset at the end of the integration time. The very low noise floor of a few electrons in modern detector arrays implies that essentially every primary particle and every secondary particle that reaches the sensitive volume of the FPA contaminates the pixels with noise charge. For example, a noise floor of 10 electrons implies that only 10 eV of energy deposition is required to generate a charge pulse equal to the noise in near-IR detectors such as HgCdTe or InSb that have ionization energies of around 1 eV/e. Since characteristic pathlengths are on the order of 10 μm, a particle with linear energy transfer of only 1 eV/μm is problematic. The small noise charges that are near the noise floor cannot be removed by signal processing.

Imaging arrays typically have non-destructive readout capability. That is, the signal charge can be sampled multiple times during the integration time without disturbing the integrated charge. This fact enables signal processing algorithms to recognize and remove the charge-contaminated pixels that have suffered a particle transient.

For example, the science mission for the Next Generation Space Telescope (NGST) includes high resolution imaging and spectroscopy in a near infrared (NIR) wavelength band with cut-off wavelength of ~5 μm, and a mid infrared (MIR) band with cut-off wavelength of ~28 μm. The requirements include a combination of very low noise (10 electrons or less) and very long integration times (hundreds to thousands of seconds). These requirements place unprecedented demands on performance with respect to transient radiation effects

This work was supported by NASA Goddard Space Flight Center under the NGST Program and the NEPP Electronic Radiation Characterization Project; and NASA Marshall Space Flight Center under a NASA Research Announcement NRA8-31 (LWS/SET).
J.C.Pickel is with PR&T, Inc., Fallbrook, CA. (jim@pickel.net)
R.A. Reed and R. Ladbury are with NASA Goddard Space Flight Center, Greenbelt, MD.
B.Rauscher is with Space Telescope Science Institute, Baltimore, MD.
P.W.Marshall is with NASA Goddard Space Flight Center, Brookneal, VA.
T.M.Jordan is with EMP Consultants, Gaithersburg, MD.
B.Fodness and G.Gee are with SGT, Inc., Greenbelt, MD.

from the space environment. A preliminary estimate is that one practical limit to signal integration times will be about 1000 seconds, set by the primary cosmic ray flux. Longer exposure time may be possible using more sophisticated cosmic ray rejection software to identify hits and continue the integration [2]. Although this approach has worked well with other space-based observatories such as Near Infrared Camera Multi Object Spectrometer (NICMOS), it has not yet been empirically demonstrated at the noise levels required for NGST. Design of rejection schemes and mission planning for effective mitigation of the cosmic ray induced noise requires a priori knowledge of the FPA response to the total particle environment, including primary, secondary and radioactive decay particles.

For the NGST program, we have defined the external ionizing particle environment and have performed Monte-Carlo transport analyses through typical spacecraft and surrounding structural material to define typical ionizing particle environments at the FPA. Concerns for very small transients and pixel-upset specifications require that the transport codes track low-energy secondary particles as well as primary particles. An array charge transport (ACT) model has been developed to predict the spatially-dependent charge contamination of the FPA on a pixel-by-pixel basis. Both the detector layer and the readout integrated circuit layer in a hybrid FPA configuration are modeled. Incident particle events, both primary and secondary, are characterized by the type of particle, energy, hit location on the surface of the FPA and angle of incidence. The charge generated in the FPA material is then distributed to the appropriate pixels to produce a pixel map of charge contamination events. The charge contamination pixel maps can be combined with pixel dark-field noise maps and imaging scenes to assess the performance impact. The modeling approach allows predictions to be made for the effect of FPA transients under various scenarios including integration time, solar weather, FPA design and spacecraft design.

In this paper, we briefly summarize the secondary particle environments and environment transport analyses, while the focus of the paper is charge collection for the array charge transport model.

2. Energetic Particle Environment

The overall transient noise problem for an optical sensor in the space environment is illustrated in Fig. 1, showing the FPA enclosed in surrounding material (packaging, telescope, spacecraft, etc.). The ionizing particle environments of concern include galactic cosmic rays (GCR) and solar-particle-event (SPE) generated protons, heavy ions, and electrons. In addition, inherent and induced radioactive sources in the material surrounding the FPA are potential sources of ionizing particles

The primary GCR particle environment in space is fairly well understood [3]. Secondary particles include delta electrons and nuclear reaction by-products.

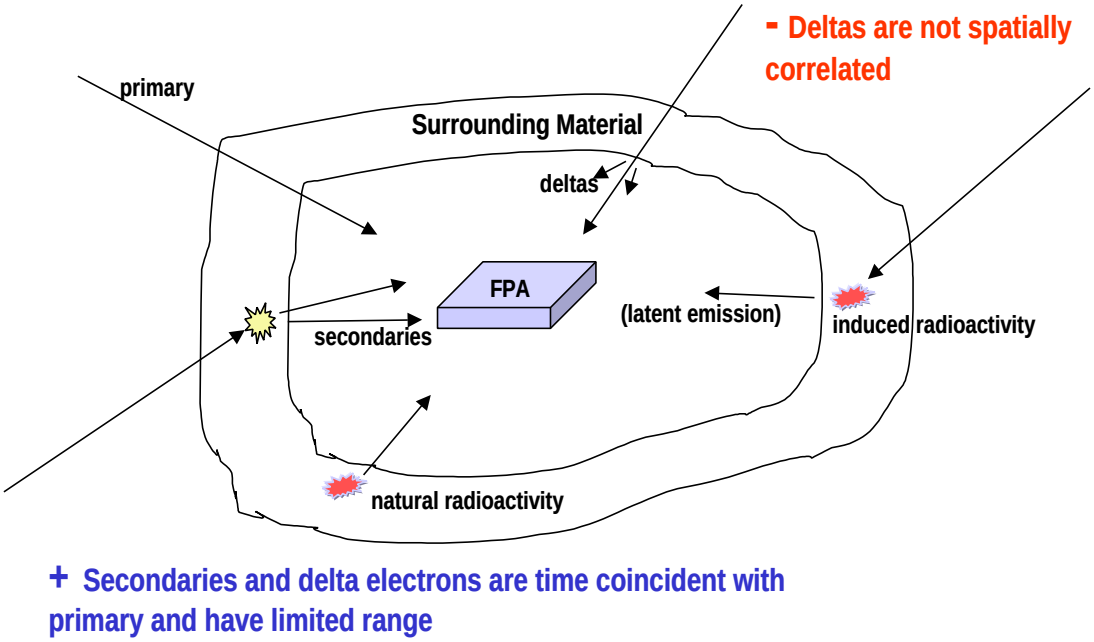

Fig. 1. Ionizing particle radiation incident on the FPA.

There is experimental evidence of secondary particles interfering with IR telescopes from the on-orbit experience of the European Space Agency's Infrared Space Observatory (ISO) [4]. Measurement of transients in the ISO detectors indicated a transient rate approximately 80 % higher than could be accounted for by the primary particles. The higher than expected transient rate was attributed to secondary particles and delta electrons.

The penetrating radiation through the spacecraft causes the structure to become radioactive by inducing nuclear reactions. The population of activated radioactive products will build up over the duration of the mission. There will be increased activation during and after solar particle events. In addition, inherent radioactive impurities contained in spacecraft materials are a source of ionization transients.

3. Array Charge Transport Model

We seek a quantitative model for ionizing particle interaction with the FPA that will serve as an engineering tool for FPA design and mission planning. The goal of the modeling is to capture only the essential physics of the charge generation and collection, such that quantitatively accurate prediction can be made for charge contamination in the FPA pixels. Because integration times are long compared to charge collection times and charges are essentially "latched" into the pixel integration nodes until reset at the end of the integration period, the modeling does not address temporal effects. We assume that the local particle environment at the FPA is described by particle type, energy, hit location on the FPA and trajectory from a separate transport analysis (not the subject of this paper).

The array charge transport modeling takes its basis from a similar approach used by Lomheim and co-workers to predict proton-induced charge deposits in charge coupled devices (CCDs) [5,6]. The model accounts for the spatial variation of charge collection in each pixel of the hybrid FPA following charge generation along the path of an ionizing particle, either electrons, protons or heavy ions. The model specifically addresses the 3-D geometry of charge collection volumes in a hybrid FPA, consisting of an array of detectors hybridized to a readout integrated circuit (ROIC) array through indium bump interconnects. Fig. 2 shows a cross-section of a typical hybrid FPA. Typical detector material for near-IR wavelengths would be HgCdTe or InSb. The substrate may be thinned or removed from the detector array to extend detection to shorter wavelength.

The model output is a pixel map of charge deposits across the FPA due to the particles that strike the FPA during the integration time. This data can then be combined with a device-dependent distribution of inherent noise to produce a simulated "dark image" file.

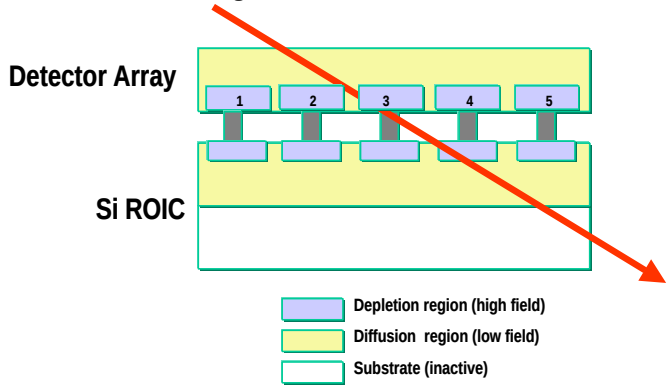

Fig. 2. Typical hybrid IR FPA geometry. A detector array is hybridized to a Si ROIC through Indium bump bonds. Charge collection due to the passage of ionizing particles occurs in both the detector array and the ROIC array.

The charge collection volumes (sensitive volumes) associated with a particular pixel are defined as those regions that collect charge to the integration capacitance for the pixel. The sensitive volumes in the photovoltaic detectors consist of the depletion volume of the p-n junction and the smaller of either a) the volume defined by the junction area and the minority carrier diffusion length in the detector active layer, or b) the pixel area and active layer thickness. The sensitive volumes in the ROIC are defined by the pixel pitch and the thickness of the Si epitaxial layer or the minority carrier diffusion length. Unless limited by wells or guardbands, the entire pixel volume of both the detector and the ROIC is sensitive to charge collection because the integration time is much longer than minority carrier lifetimes.

A key concern is charge spreading to adjacent pixels from the pixel that is penetrated by the particle, i.e., radiation transient crosstalk. Charge spreads by diffusion in both the detector array and the ROIC array. Mechanisms for charge spread by diffusion in the detector array are obvious since detector arrays are designed to collect photo-generated charge by diffusion from the active region with maximum efficiency. High density staring arrays typically do not have distinct charge separation barriers between the pixels. Instead, they rely on pixel geometry and slight electric fields from doping gradients to nudge the charge toward the local pixel junction. In all ROIC unit cells, a reset MOSFET is required to reset the integration capacitor and the junction that is connected to the integration capacitor is a sensitive charge collection junction. Charge collected on the sensitive junction is transported to the integration capacitor. The integration time is long compared to minority carrier diffusion times. Thus, all charge that diffuses from the ion path to any

sensitive junction in the ROIC will be collected and counted to the respective pixel. In order to accurately model the charge collection by diffusion, the field-assisted drift component associated with the MOSFETs, and perhaps built-in fields in the diffusion regions of the detectors, needs to be taken into account. Similar considerations for charge spreading by diffusion apply to CCD, active pixel sensor (APS) and photovoltaic (PV) detector technologies.

The modeling task is to calculate charge generation along the 3-D path of the particle and follow the generated minority carriers until they are collected on a pixel integration node or recombine. For the current version of the model, we are not addressing temporal variation of charge collection since integration times are typically much longer than charge collection times. The final result is a spatial mapping of charge collection across the array during the integration time.

Fig. 3 illustrates the general approach taken in the array charge transport model. For illustration, only the depletion and free-field diffusion layers of the detector are shown. In the actual model, the depletion and diffusion layers are further subdivided into regions with offsets from the pixel edges representing junctions and wells, providing a fully 3-D description of the structure. In addition, spatially dependent electric fields may exist that require consideration for drift-assisted diffusion. Such a modeling approach can be applied to any detector structure, including hybrid FPAs, integrated active pixel sensors (APS) and CCDs, by registering the various layers on the Cartesian coordinate system and propagating the particle trajectory through the structure.

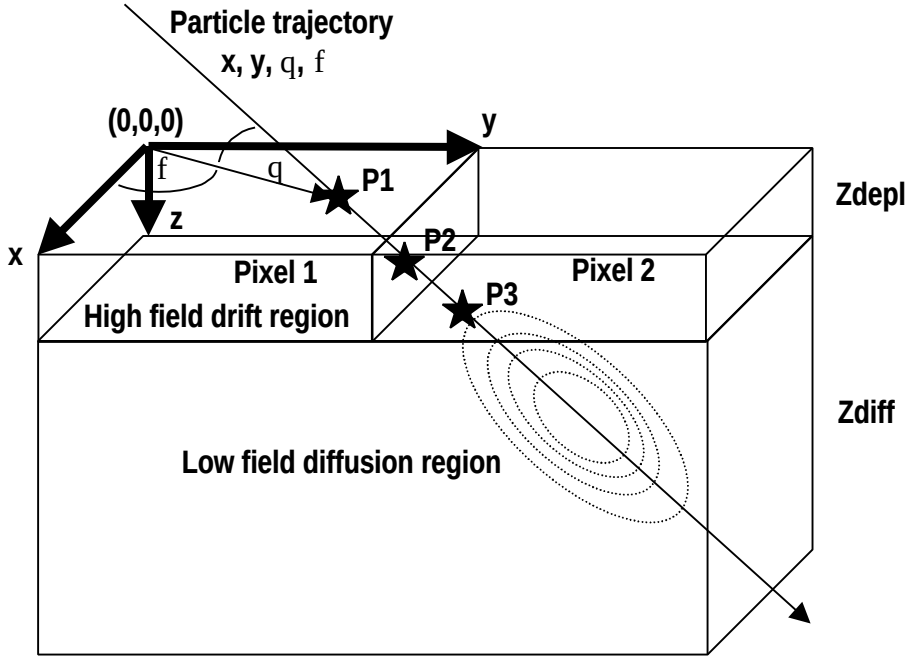

Fig. 3. Simplified illustration of Array Charge Transport model. A particle passes through depletion regions in pixel 1 from P1 to P2, and pixel 2 from P2 to P3 and then passes into the common substrate diffusion region.

The radiation source terms for the charge collection model are derived from the external particle environment transported through the material surrounding the FPA. The output of the transport analysis is a list of particles incident on the FPA during the integration time. The particles include both primary and secondary particles and are described with attributes as listed in Table 1.

Table 2 lists the primary attributes of the FPA that determine the charge collection characteristics. The particle type and energy determine the linear energy transfer (LET). From the ionization energy for the target material, W, we determine the charge generation rate, linear charge transfer (LCT), in carriers/μm. Recombination of carriers is taken into account by assigning an effective diffusion length, L. As the particle loses energy to the target material, the energy decreases and the LET changes. The model accounts for this effect by recalculating the energy after each path increment based on the TRIM code [7].

Assumptions and Simplifications

The modeling goal is to determine the final spatial charge distribution across the array. Since noise levels on the order of 10 electrons are of concern, we are operating at levels much lower than are normally considered for

radiation effects analysis. An exact accounting of the fate of each free carrier generated in a large array (typically 2k x 2k pixels, or larger) during the integration period is not computationally practical. Thus, we make several simplifying assumptions and utilize a combination of modeling approaches, including Monte Carlo techniques for particle hits and a combination of analytical and Monte Carlo solutions to charge collection.

TABLE 1. INCIDENT PARTICLE ATTRIBUTES

Parameter	Symbol	Characteristics
Impact Position	X,Y	Random
Trajectory	?,f	Isotropic
Particle	Z,A	Depends on primaries, secondaries, radioactive decay
Energy	E	Conforms to energy spectrum at FPA after transport
Stopping Power	LET	Depends on Z, E
Range	R	Depends on Z,E

TABLE 2. FPA ATTRIBUTES

Parameter	Symbol	Characteristics
Material	InSb, HgCdTe or Si	Determines ionization: W, LCT
Pitch		Determines pixel geometry
Depletion Width and Pixel Offsets	Zdepl	Charge collection by drift
Diffusion Width and Pixel Offsets	Zdiff	Charge collection by diffusion
Spatially Variant Electric Field	E(r)	Charge collection by drift-assisted diffusion
Diffusion Length	Ldiff	Recombination-limited diffusion

The path of high energy protons and heavy ions is assumed to be a straight line through the FPA, defined as an array of detector pixels geometrically registered to an array of ROIC unit cells, with trajectory determined by the initial angle of incidence (?,f) and point of impact (x,y). This assumption is justified since the ions are deviated from their path only by nuclear scattering and this is low probability in the small dimensions of the FPA.

However, the path of energetic electrons is not necessarily straight. The small mass of electrons can result in large angle scatters from collisions with bound electrons in the target material. To account for the zigzag path of the electrons, we use the Monte Carlo routines in the NOVICE code [8].

Each particle has a residual range that is determined by its energy. If a particle range is less than the remaining distance within the current pixel, the particle energy and resulting charge is assumed to be deposited at that point.

Energetic secondary electrons (delta electrons) are generated along the path of protons or heavy ions by Coulombic interactions that transfer energy to electrons in the target material. The delta electrons are a source of further ionization and charge deposition. We account for delta electron generation within the interior of the FPA assembly (active side of detector, interconnecting Indium bump-bonds, and active side of ROIC) with a source generation function pre-calculated with the NOVICE code for each material of interest.

Secondary particle production from nuclear scattering is neglected since the probability is small.

Energy deposition is determined by LET and pathlength. LET is converted to LCT (e/um) by the ionization energy, W, for the target material. For HgCdTe and InSb with 5 μm cutoff wavelength, W is ~1 eV per carrier pair (eV/cp). For Si W is ~3.8 eV/cp at cryogenic temperature.

Charge Collection

We are using a hybrid approach to charge collection. The initial line source of minority carrier distribution along the particle path depends on the particle LET, hit location (x,y) and trajectory (?,f). The final disposition of the carriers depends on the geometry and spatially-dependent minority carrier diffusion and drift. Particle history ends when it is either collected on a pixel node or recombination occurs. Charge collection is by drift, diffusion or a combination of drift and diffusion. We use different charge collection modeling approaches, depending on the local electric field in the current region along the pathlength.

Charge Collection by Drift

Charge generated within a high electric field region is transported by drift and we assume 100% collection efficiency to the associated pixel. High field collection regions could include depletion regions of p-n junctions in photovoltaic detectors or high field region in impurity band conduction Si detectors. Charge collection in the depletion region is given by

$$Q_{depl} = LCT * R_{depl} \quad (1)$$

where LCT is linear charge transfer (e/um), and R_{depl} is the pathlength in the depletion region.

Charge Collection by Diffusion

Charge generated in zero or low electric field regions is transported to the depletion/diffusion boundary by diffusion. Any charge that reaches the depletion/diffusion boundary is assumed to be collected on the associated pixel. We use an analytical solution to the 3-D diffusion equation that was developed by Kirkpatrick [9] to

calculate the geometric distribution of charge to the pixel regions, similar to the approach used by Lomheim [5,6]. The Kirkpatrick model solves the 3-D diffusion equation for a point source, $Q_{ps}(x,y)$, at (x,y) coordinates on the depletion/diffusion interface plane. Boundary conditions assume a semi-infinite medium and recombination-limited diffusion length is not included. $Q_{ps}(x,y)$ gives the charge per unit area at the depletion/diffusion boundary from a point source inside the diffusion region. Integration of $Q_{ps}(x,y)$ along the ion trajectory, (?,f), for a chosen length, L, provides the surface charge density at the depletion/diffusion boundary due to a line source, $Q_{ls}(x,y,?,f ,L)$.

$Q_{ls}(x,y,?,f ,L)$ is then numerically integrated over the pixel areas at the depletion/diffusion boundary to give the charge collected to each pixel (m,n) in the array as

$$Q_{diff(m,n)} = ?? Q_{ls}(x,y\ ?,f\ ,L)dxdy \qquad (2)$$

We can account for spatially variant recombination-limited diffusion length by differencing the calculations along the trajectory and varying L appropriately.

Charge Collection by Field-Assisted Diffusion

The transport space is not uniform and some regions may have built-in fields due to doping gradients, variable fields due to device biasing, and spatial variation of minority carrier lifetime. For these intermediate field regions, we account for field-assisted diffusion. That is, the carriers will diffuse from their origin according to normal diffusion processes but there will be a drift bias that preferentially moves the diffusing charge cloud in the direction of the electric field. Here we use a hybrid Monte Carlo solution to the transport equation relating particle density to diffusion and drift.

We follow an approach first proposed by Sai-Halasz for simulating alpha particle single event effects in integrated circuits [10]. Rather than simulate the actual motion of the carriers, we simulate the simplest process that still follows, in average, the drift and diffusion processes described by the transport equation. A 3-dimensional random walk is used with spatially dependent drift. For a diffusion length, L, a step, L_r, is randomly selected between –L and +L. Then the particle's x coordinate is replaced by $x+L_r$. The same process is applied to the y and z coordinates and the cycle repeats for another particle.

Following Sai-Halasz, the time for the particle to move the random diffusion step, L_r , is given by

$$t_s = L_r^2 / 18\ D \qquad (3)$$

where L_r is the diffusion step size and D is the diffusion coefficient.

If an electric field is present, a drift in the direction of the field will proceed concomitantly with the random diffusion step. The size of the drift step, $L_d(r)$, associated with each random diffusion step is given by the drift velocity and drift time, yielding

$$L_d(r) = (e\ E(r) / 18\ k\ T)\ L_r^2 \qquad (4)$$

where T is temperature, k is Boltzmann's constant and E(r) is the local electric field. The total step is then given by Lr + Ld and the appropriate step value is added to each dimension. The process repeats until the particle reaches either a collection surface such as a depletion region boundary, a recombination surface, a reflection surface, or until the lifetime-limited diffusion length is reached.

Reflection and recombination surfaces can be treated with the pseudo Monte Carlo approach described above by randomly assigning a reflection coefficient in accordance with the surface recombination velocity. This can be important for detectors at the boundary between the active layer and the substrate, which may be a partially reflecting surface to maximize optical response, and at the detector surface where there may be a high density of recombination sites due to incomplete surface passivation.

Implementation

The device geometry is described by pixel pitch and layers (e.g., detector, ROIC, indium bump) on a Cartesian coordinate system. Depletion region and diffusion region thicknesses are defined and the boundary of regions within the pixel are defined. A particle is incident on the top surface of the device with a random location and random angle of incidence. The particle type and energy determine the LET and thus the LCT. A subarray (11 pixels x 11 pixels) is defined around the hit pixel. The primary particle traverses through the layers in a straight path along the trajectory and the appropriate charge collection model is applied, depending on the type of region – either depletion (high electric field), diffusion (low electric field), drift/diffusion (moderate electric field), or recombination (dead layer or recombination surface). Diffusion length is limited by recombination lifetime. The charge generated along the particle path is partitioned to the appropriate pixels in the subarray. The process is repeated for a large number of particle hits and the subarray results for each hit are accumulated in a large array (100 pixels x 100 pixels). A noise model is used to generate a noise floor that is added to the data across the array. The large array is of sufficient size to capture all of the statistical features of the interactions. A full image

can be built up from stitching together multiple 100x100 arrays. The model is coded in Visual Basic and integrated with Microsoft Excel. The code has a Windows-based graphical user interface.

5. Discussion and Example Results

Fig. 4 shows typical simulation results for charge collection from single ion hits. Charge collection in a 10x10 array of Si volumes with 1 μm depletion width, 20 μm diffusion width and 30 μm pitch is shown for two ion cases, 20 MeV proton and 200 MeV Fe. The ion hit is near the center of the array and the angle of incidence is 60 degrees, going from back to front in the picture. Charge is collected by drift in the depletion region of the hit pixel to give a peak. Charge is collected to adjacent pixels by diffusion.

Fig. 5 shows model results for the charge collected in individual pixels after a hit to a center pixel (5,5) of a 10x10 Si array with 30 μm pitch, 1 μm depletion thickness and 10 μm diffusion thickness. The particle is a 20 MeV proton incident at 80 degrees going from top to bottom in the picture. The top array shows the charge collected from the depletion region, the center array shows the charge collected from the diffusion region and the bottom array shows the total charge. Note the charge spread across the array, particularly in the pixels along the wake of the ion track. Depletion charge is collected only in the hit pixel. All of the other pixels are collecting charge by diffusion.

Calibration of model parameters

The model contains many adjustable parameters, and it is important to calibrate these parameters with experimental data. Because the secondary particle environment is strongly dependent on the exact material and geometric configuration around the "flight" FPA and the primary particle spectrum on-orbit, it is generally not practical to test for the secondary environment. Our strategy is to calibrate the models with the primary particles and extrapolate the effects of the secondary environment with the calibrated models and detailed transport analysis. A key advantage of detailed modeling and simulation tools as described here, over simpler models that merely account for average behavior, is that aggregate behavior for a large number of hits can be studied in statistically significant quantities. These results can then be compared to measured data from space, and to controlled experiments at ground-based accelerator testing to calibrate model parameters.

Studying pulse height distribution is one method of comparing model results to experiment and inferring model parameter values. The maximum and average charge pulses in the distribution are related to the maximum and average pathlength, respectively, in the charge collection volume, which in turn are related to

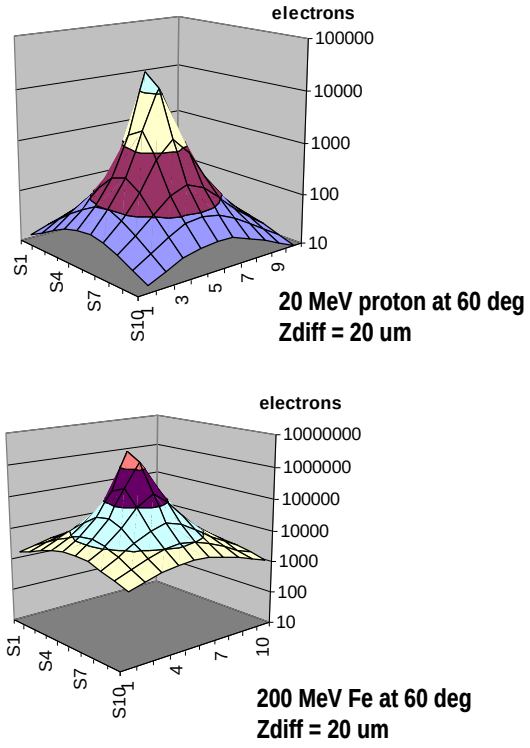

Fig. 4. Charge collection in 10x10 array of Si pixels on 30 μm pitch with 1 μm depletion thickness and 10 μm diffusion thickness. Two ion cases are shown.

20 MeV proton at 80 deg, Zdiff = 10 um

0	0	0	0	0	0	0	0	0	0	
0	0	0	0	0	0	0	0	0	0	DEPLETION
0	0	0	0	0	0	0	0	0	0	
0	0	0	0	0	0	0	0	0	0	
0	0	0	0	7424	0	0	0	0	0	
0	0	0	0	0	0	0	0	0	0	
0	0	0	0	0	0	0	0	0	0	
0	0	0	0	0	0	0	0	0	0	
0	0	0	0	0	0	0	0	0	0	
0	0	0	0	0	0	0	0	0	0	

7	8	11	12	13	12	10	8	6	5	
9	13	18	23	24	22	18	13	9	7	DIFFUSION
14	22	34	49	56	48	33	21	14	9	
20	36	70	137	195	135	68	35	19	11	
26	55	145	585	20881	550	140	54	25	14	
30	71	236	1814	30406	1643	225	69	30	15	
30	70	229	1656	13432	1510	218	68	29	15	
25	53	132	416	882	399	127	51	25	14	
19	33	62	111	142	109	61	33	18	11	
13	20	31	42	48	42	30	20	13	8	

7	8	11	12	13	12	10	8	6	5	
9	13	18	23	24	22	18	13	9	7	TOTAL
14	22	34	49	56	48	33	21	14	9	
20	36	70	137	195	135	68	35	19	11	
26	55	145	585	28305	550	140	54	25	14	
30	71	236	1814	30406	1643	225	69	30	15	
30	70	229	1656	13432	1510	218	68	29	15	
25	53	132	416	882	399	127	51	25	14	
19	33	62	111	142	109	61	33	18	11	
13	20	31	42	48	42	30	20	13	8	

Fig. 5. Charge collected in depletion and diffusion arrays is combined for the total charge array. Charge to the hit pixel is collected by drift and charge to other pixels is collected by diffusion.

the geometry of the collection volume. Fig. 6 shows pulse height distribution simulation results for a 100x100 pixel HgCdTe detector array with 20 µm pitch, 1 µm depletion layer and different diffusion layer thicknesses. The particle LCT is constant at 1000 e/µm, consistent with GeV range protons in 5µm cutoff HgCdTe. The simulation is for 300 hits, randomly located and with random trajectory, as would be the case for exposure in space. The high end of the distribution is due to the primary hits and the low end of the distribution is due to charge spread (crosstalk) to neighboring pixels. The average pulse amplitude and maximum pulse amplitudes for the primary hits are consistent with expectations from simple models that calculate average and maximum pathlength in a rectangular parallelepiped. The degree of crosstalk increases with increasing diffusion layer thickness as expected.

Fig. 7 shows pulse height distributions for simulation of 30 MeV proton hits to HgCdTe detectors with the same pitch and layer thicknesses as discussed in Fig.6. In this case, we are simulating an accelerator test and have 100 proton hits randomly located across the 100x100 array but all with 60 degree incidence. Note the different slopes of the distribution in the lower energy tails. The slope decreases with increasing diffusion layer thickness. Such simulation information can be combined with test data to infer an effective diffusion layer thickness.

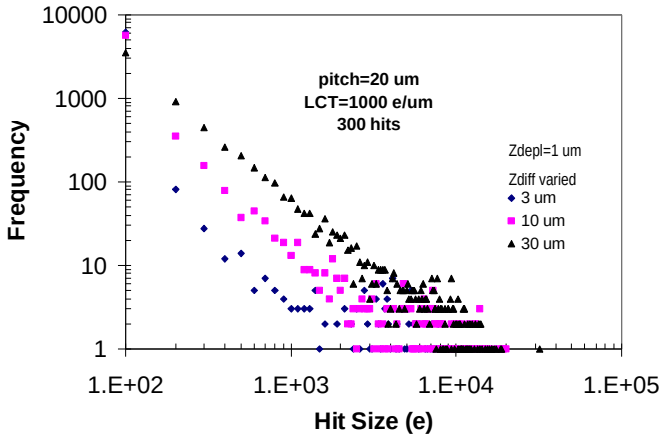

Fig. 6. Pulse height distribution simulation results for 300 hits to 20 µm pitch, 100x100 array of HgCdTe detectors. The particles simulate GeV-range protons with omni directional incidence.

Fig. 8 shows model predictions of crosstalk to the nearest neighboring pixels for the case of a 30 µm pitch Si pixel struck in the center with an ion at normal incidence. Crosstalk is a function of both pitch and diffusion layer thickness. When omni directional hits and random hits within the pixel area are considered, the crosstalk is larger.

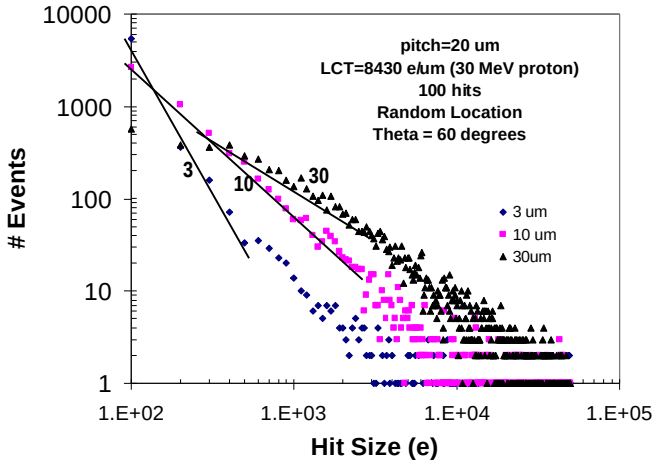

Fig. 7. . Pulse height distribution simulation results for 100 hits to 20 µm pitch, 100x100 array of HgCdTe detectors. The particles simulate 30 MeV protons with 60 degree angle of incidence.

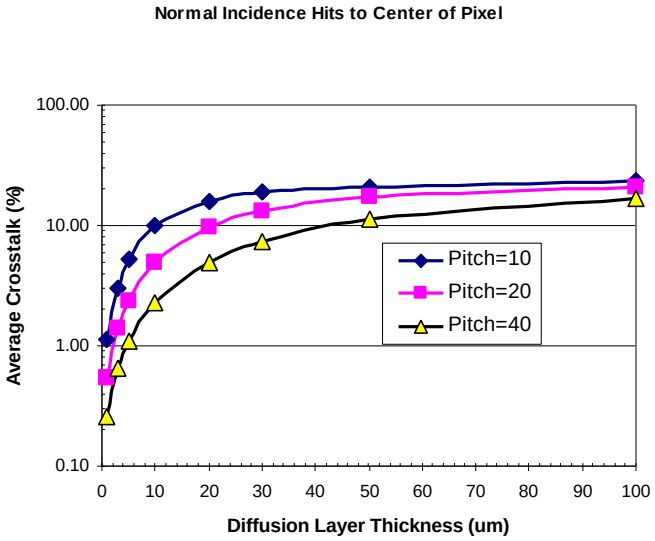

Fig. 8. Model predictions of crosstalk as a function of diffusion layer thickness and pixel pitch.

Comparison to NICMOS Data

After considerable data processing and interpretation, on-orbit data from a HgCdTe FPA in the NICMOS camera on the Hubble Space Telescope provides a rich data source for cosmic ray induced transients [11]. Fig. 9 shows an observed pulse height distribution from dark field images from NICMOS taken outside of the South Atlantic Anomaly (SAA). The NICMOS environment outside of SAA consists mostly of GeV-range protons. The magnetosphere has filtered out lower energy particles, leaving a nearly mono-LET source of omni directional protons with LCT of ~1200 e/um in the HgCdTe detector array. See Reference 11 for details. The simulation assumes a 40 um pitch with a 1 um depletion layer thickness and a 5 um diffusion layer thickness. The results are for 300 primary hits.

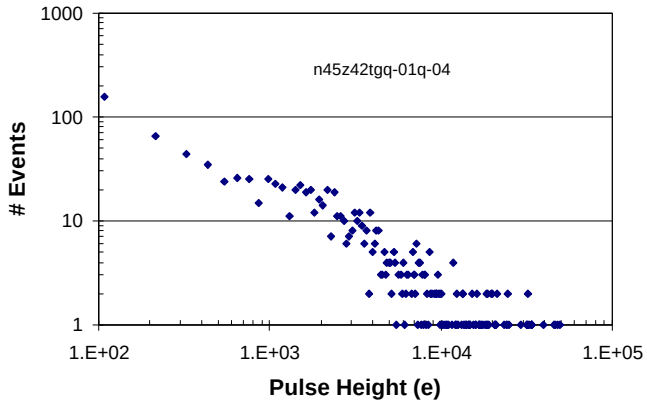

Fig. 9. Pulse height distribution observed on-orbit for NICMOS (after data processing).

Fig. 10 shows model simulation of the pulse height distribution for the NICMOS conditions shown in Fig 9. Secondary particles are not included in the simulation. The LCT is 1200 e/um and hits are random in location and trajectory. The larger pulses in the spectrum are due to the primary hits. The lower energy tail is due to crosstalk. We see good agreement on the primary particle hit amplitudes and general qualitative agreement on the shape of the distribution. There are more low amplitude pulses in the simulation than were observed in the data.

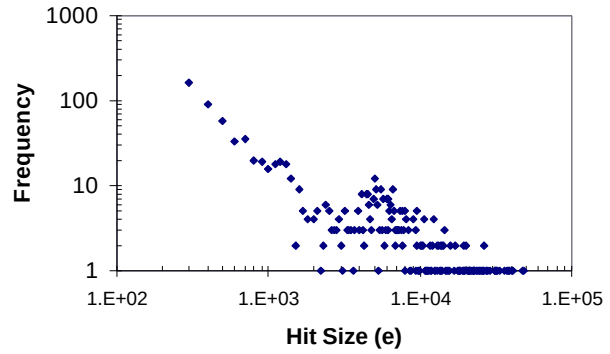

Fig. 10. Model prediction for NICMOS pulse height distribution. The distribution includes 300 primary hits with random location and trajectory on a 100x100 array.

Comparison to APS Data

Heavy ion tests on an Active Pixel Sensor (APS) test chip also provide a source of data for validating the charge collection aspects of the model [12]. In Fig. 11, we compare model simulations to test data for 600 MeV Ar hits to an APS test chip. The APS test chip is a 256x256 Si photodiode array and is separated into 4 quadrants of 128x128 pixels [13]. The pixel pitch is 16.2 μm. Each quadrant has a different pixel design that affects the charge collection characteristics. Consequently there was large variation in the response to heavy ion hits for each of the quadrants [12]. In Fig. 11, we show test data for a 600 MeV Ar hit to quadrant 1 (left figure) and quadrant 2 (middle figure). The data saturates at 1700 DN (digital number) counts. The simulation is shown as the right figure, with artificial saturation imposed at 1700 DN. The simulation assumed a 1 μm depletion layer thickness and 25 μm diffusion layer thickness, with both layers covering the entire pixel area. In both the data plots and the simulation plot, an 11x11 array is centered around the ion hit at normal incidence.

Qualitatively, the simulation results are intermediate between the quadrant 1 and quadrant 4 data. We see general agreement on the gross characteristics of the charge spread. Compared to the simulation, quadrant 1 has a more focused charge collection and quadrant 2 has a less focused charge collection. The actual charge collection volumes within the pixel are much more complex than the simple depletion layer on a diffusion layer that was assumed for the simulation, and the electric fields within the structure probably modify the diffusion characteristics beyond the simple free-field diffusion assumed in this simulation. The intent of this analysis was to reproduce the gross features of the data. A more comprehensive analysis that takes the detailed pixel charge collection structures into account will be performed in the future.

6. SUMMARY

We have presented charge collection models and a structured approach for simulating ionizing particle interactions with detector arrays. The modeling uses a combination of analytical and Monte Carlo techniques to capture the essential features of charge collection to the detector pixels. The model addresses several aspects that are necessary for high fidelity simulation of complex FPA structures including multiple layers, sub-regions within layers, variation of LET with range, secondary electron scattering, free-field diffusion, and field-assisted diffusion. Methodology for calibration of model parameters with experimental data were discussed, and comparison of simulation predictions to available data was presented. Future work will compare model predictions to data and calibrate model parameters based on an extensive set of test data obtained on state-of-the-art FPA technologies on the NGST Program. While the paper concentrated on infrared detector arrays, the simulation methodology and modeling tools can be applied to any semiconductor detector array to predict radiation-induced charge collection .

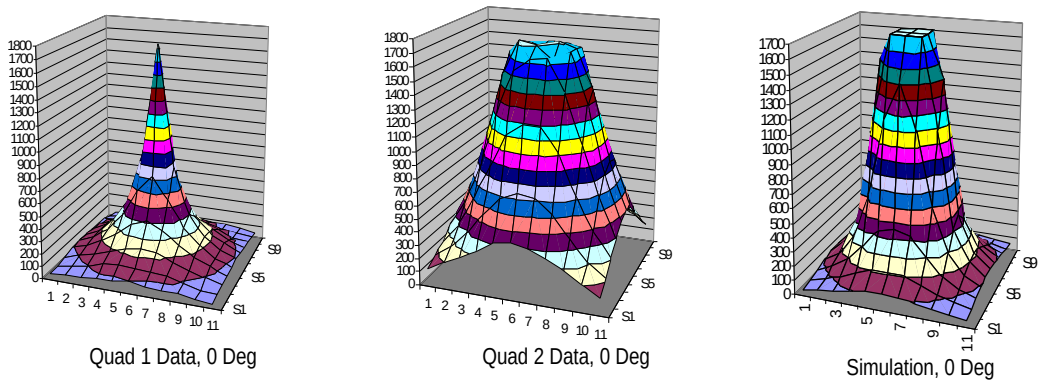

Fig. 11. Ar ion hits at 0 degrees on 2 quadrants of Active Pixel Sensor test chip compared to model simulation.

REFERENCES

[1] A.Fowler, T.Greene, M.Greenhouse, D.Hall, K.Long, J.MacKentry, B.Martineau, C.McCreight, J.Pipher, M Ressler and E.Young, "Recommendations of the NGST Detector Requirements Panel," NGST Document 641, October, 1999.

[2] Offenberg et al. 1999, "Cosmic Ray Rejection Aboard the NGST," in ASP Conference Series, "Astronomical Data Analysis Systems and Software VIII," in press.

[3] J.L.Barth, J.C. Isaacs, and C. Poivey, "The Radiation Environment for the Next Generation Space Telescope," NGST Document 570, September 2000.

[4] A.Claret, H.Dzitko and J.J.Engelmann, "Transient Particle Effects on the ISOCAM Instrument On-Board the Infrared Space Observatory," IEEE Trans. Nucl. Sci., Vol. 49, No. 6, p. 1511, December 1999.

[5] T.S.Lomheim, R.M.Shima, J.R.Angione, W.F.Woodward, D.J.Asman, R.A.Keller and L.W.Schumann, "Imaging Charge-Coupled Device (CCD) Transient Response to 17 and 50 MeV Proton and Heavy Ion Irradiation," IEEE Trans. Nucl. Sci., Vol. 37, No. 6, p. 1876, December 1990.

[6] T.E.Dutton, W.F.Woodward and T.S.Lomheim, "Simulation of Proton-Induced transients on Visible and Infrared Focal Plane Arrays in a Space Environment, SPIE, Vol. 3063, p.77, 1997.

[7] J.F.Ziegler, J.P.Biersack and U.Littmark, "The Stopping and Range of Ions in Solids," Pergamon Press, 1985.

[8] T.M.Jordan, "An Adjoint Charged Particle Transport Method," IEEE Trans. Nucl. Sci., Vol. 23, 1976.

[9] S.Kirkpatrick, "Modeling Diffusion and Collection of Charge from Ionizing Radiation in Silicon Devices," IEEE Trans. Elec. Dev., Vol. ED-26, p. 1742, 1979.

[10] G.A.Sai-Halasz and M.R.Wordeman, "Monte Carlo Modeling of the Transport of Ionizing Radiation Created Carriers in Integrated Circuits," IEEE Elect. Dev. Lett., Vol. EDL-1, No. 10, p. 211, October 1980.

[11] R.Ladbury, J.C.Pickel, G.Gee, T.M.Jordan, L.Bergeron, B.Raushcer, R.A.Reed, P.W.Marshall, D.Figer and B.Fodness, "Characteristics of the Hubble Space Telescope's Secondary Radiation Environment Inferred from Charge Collection Modeling of Near Infrared Camera and Multi-Object Spectrometer," this conference.

[12] P.W.Marshall, W.B.Byers, C.Conger, E.Eid, G.Gee, M.R.Jones, C.J.Marshall, R.A.Reed, J.C.Pickel, S.Kniffen and J.Peden, "Heavy Ion Transient Characterization of a Photobit Hardened-by-Design Active Pixel Sensor Array," this conference.

[13] E.S.Eid, T.Y.Chan, E.R.Fossum, R.H.Tsai, R.Spagnuolo, J.Deily, W.B.Byers,Jr. and J.Peden, "Design and Characterization of Ionizing Radiation-Tolerant CMOS APS Image Sensors up to 30 Mrd(Si) Total Dose," IEEE Trans. Nucl. Sci., Vol. 48, No. 6, p. 1796, December 200